

# GEM: A Dynamic Tracking Model for Mesoscale Eddies in the Ocean

Qiu-Yang Li<sup>1</sup>, Liang Sun<sup>1,2</sup>, Sheng-Fu Lin<sup>1</sup>

<sup>1</sup>School of Earth and Space Sciences, University of Science and Technology of China, 230026, Hefei, China.

<sup>2</sup>State Key Laboratory of Satellite Ocean Environment Dynamics, Second Institute of Oceanography, State Oceanic Administration, Hangzhou, 310012, PR China.

*Correspondence to:* L. Sun ([sunl@ustc.edu.cn](mailto:sunl@ustc.edu.cn))

## Abstract

Genealogical Evolution Model (GEM) is an efficient logical model used to track dynamic evolution of mesoscale eddies in the ocean. It can distinguish different dynamic processes (e.g., merging and splitting) within a dynamic evolution pattern, which is difficult to accomplish using other tracking methods. To this end, GEM first uses a two-dimensional (2-D) similarity vector (i.e. a pair of overlap rates) rather than a scalar to measure the similarity between eddies, which effectively solves the “missing eddy” problem (temporally lost eddy in tracking). Second, GEM uses both parents (a new eddy) and children (e.g., splitting eddies from parent eddy) in tracking, and the dynamic processes are described as birth and death of different generations. Additionally, a look-ahead approach with selection rules effectively simplifies computation and recording. All of the computational steps are linear and do not include iteration. Given the pixel number of the target region  $L$ , the maximum number of eddies  $M$ , the look-ahead time steps  $N$ , and the total number of time steps  $T$ , the total computation complexity is  $O(LM(N+1)T)$ . The tracking of each eddy is very smooth because we require that the snapshots of each eddy on adjacent days overlap one another.

Although eddy splitting or merging is ubiquitous in the ocean, they have different geographic distribution in the Northern Pacific Ocean. Both the merging and splitting rates of the eddies are high, especially at the western boundary, in currents and in “eddy deserts.” GEM is useful not only for satellite-based observational data but also for numerical simulation outputs. It is potentially useful for studying dynamic processes in other related fields, e.g., the dynamics of cyclones in meteorology.

## 29 1 Introduction

30 Eddies are ubiquitous in the ocean, and they move from one place to another [Chelton and Schlax, 1996; Chelton et  
31 al., 2007]. Eddies in the ocean can cause large-scale transports of heat, salt and other tracers [Bennett and White,  
32 1986; Chelton et al., 2011a; Dong et al., 2014; McGillicuddy et al., 2011] by trapping these passive tracers inside the  
33 eddies. Such transports may have important impacts on the environment and climate of the ocean [Dong et al., 2014].  
34 To address various applications in the studies that use satellite products of sea level anomaly (SLA) data [e.g.,  
35 Chelton et al., 2011b] and numerical simulation outputs [e.g., Petersen et al., 2013], oceanic eddies should be  
36 automatically recorded using these data and outputs [e.g., Yang et al., 2013; Sun et al., 2014; Pegliasco et al., 2015].  
37 In general, the recording of oceanic eddies often includes two independent steps: automated eddy identification and  
38 automated eddy tracking. The eddies are identified in a sequence of SLA maps using an identification algorithm or  
39 identified from velocity fields. An automated tracking procedure is then applied to determine the trajectory of each  
40 eddy [Chelton et al., 2011b]. Several automated identification and tracking algorithms have been developed for  
41 eddies in the ocean [Chelton et al., 2011b; Ienna et al., 2014; Mason et al., 2014; Yi et al., 2015].

42 For the eddy tracking stage, according to a recent census [Wang et al., 2015; Yi et al., 2015], approximately 10-30%  
43 of eddies may be found in proximity to a neighboring eddy in any given global SLA map and they frequently  
44 interact. Therefore, an eddy tracking process should have the capability to distinguish different dynamic processes  
45 (e.g., merging and splitting) during its dynamic evolution. Moreover, an eddy tracking process must be accurate and  
46 fast enough to handle a huge amount of data, which will be even larger in size if spatio-temporal resolution of  
47 observations and numerical simulations increases.

48 Implemented automated tracking procedures differ in detail, but they are all similar in concept because they utilize  
49 the nearest neighbor strategy [Chelton et al., 2011b]. For each eddy  $E_i$  identified at time step  $k$ , the nearest eddy to  $E_i$   
50 at the next time step  $k+1$  is identified as part of the trajectory of eddy  $E_i$ . A more advanced procedure uses eddy  
51 shape error as an additional condition when assessing an eddy trajectory [Mason et al., 2014].

52 However, there is a “missing eddy” problem that must be solved in the eddy tracking stage [Chelton et al., 2011b].  
53 An eddy at time step  $k$  may have no associated eddy at time step  $k+1$ , which is simply due to a temporary missing  
54 eddy in the identification process; this can occur for a variety of reasons related to sampling errors and measurement  
55 noises [Chelton et al., 2011b] or limitations of the eddy detection step when an eddy is too weak/small at a time step.  
56 Chelton and his colleagues made an attempt to accommodate such problems; they allowed for the reappearance of a  
57 temporarily missing eddy by looking ahead two or three time steps. Unfortunately, this “look-ahead” procedure  
58 considers too many nearby eddies as potential ones. In practice, the results of this simple “look-ahead” procedure  
59 were disappointing because the resulting eddy trajectory often jumped from one eddy track to another. As a result,  
60 the look-ahead approach was abandoned, even though it is [Chelton et al., 2011b].

61 Recently, the concept of Multiple Hypothesis Assignment (MHA) was introduced to solve the missing eddy problem  
62 by abandoning the simple closest eddy strategy and applying a new “look-ahead” procedure [Faghmous et al., 2013].  
63 The MHA method can effectively solve the missing eddy problem in a straight-line model when the following

64 trajectory being followed is a branch without any splitting, but it is algorithmically and computationally complex.  
65 Given the maximum number of eddies in any time frame  $M$ , the number of look-ahead time steps  $N$  (with  $N=0$  being  
66 the original linear closest eddy procedure without look-ahead) and the total number of time steps  $T$ , the MHA has a  
67 larger computational complexity (the total amount of time taken by an algorithm),  $O(M^{N+1}T)$  at the worst-case  
68 [Faghmous et al., 2013]

69 The existing straight-line model can trace the kinematic motion of eddy. The dynamic evolutionary processes (e.g.,  
70 merging and splitting) of the eddy are, however, ignored by the model. This implies that each eddy  $E_i$  identified at  
71 time step  $k$  has only one eddy as part of its trajectory at time step  $k-1$  and has only one eddy as part of its trajectory  
72 at time step  $k+1$ . In the ocean, small eddies may merge to form larger ones. As shown in Figure 1, the anticyclonic  
73 eddies AC1 and AC2 observed on July 26, 2006 merged into a single one on July 31, 2006. Then, the cyclonic  
74 eddies C1 and C2 on July 26, 2006 merged to form a larger one on August 3, 2006. To describe such processes, the  
75 eddy tracking records should be trees with branches instead of simple straight lines.

76 To record the dynamic evolution of eddies, two fundamental algorithms are required. First, the two nearby eddies  
77 should be distinguished in the identification stage using a segmentation strategy in which the target region is divided  
78 into two corresponding eddies. Otherwise, the merging and splitting processes cannot be determined properly. This  
79 problem was recently solved by the use of segmentation strategies, e.g., the close-distance segmentation strategy [Li  
80 et al., 2014] and the watershed strategy [Li and Sun, 2015]. Because these segmentation strategies can distinguish  
81 closed eddies, they can also potentially reduce the risk of having a missing eddy in the identification process.

82 Second, the merging and splitting processes in the tracking stage should be described in detail. We use a multi-  
83 branch tree model to do so. The eddy  $E_i$  identified at time step  $k$  may arise from more than one eddy at time step  $k-1$ ,  
84 which subsequently merged; and  $E_i$  may become more than one eddy at time step  $k+1$  if it splits. We refer to this  
85 model as the “Genealogical Evolution Model (GEM)” because it is a genealogical tree for recording the whole  
86 evolutionary history of an eddy. The multi-way tree model in computer science can be used to store this type of  
87 structure.

88 Moreover, the GEM also provides a new way to solve the missing eddy problem. Instead of the existing closest eddy  
89 strategy, a temporal track tree with  $N$  look-ahead time steps is used to maintain all possible tracks with the help of  
90 the multi-way tree model. The method can effectively solve the missing eddy problem, regardless of whether the  
91 eddy is splitting or not.

92 In this paper, we introduce the GEM to describe mesoscale eddies in a tracking process with a total number of time  
93 steps  $T$ . The GEM allows the eddy to have multiple eddies as its parents or as its children in a multi-branch model. It  
94 also solves the missing eddy problem by using a new look-ahead method similar to the MHA. Compared with the  
95 computational complexity  $O(M^{N+1}T)$  of MHA, the new method is much faster and has much less computational  
96 complexity  $O(LM(N+1)T)$ , where  $L$  denotes the pixels of target region. Besides, if the GEM was implemented with  
97 the computer codes properly the output data of GEM also record the dynamic evolution of the eddy in detail and will

98 potentially be useful for other research fields, e.g., the dynamics of cyclones in meteorology. As an example, The  
99 GEM is applied to eddies in the North Pacific Ocean (NPO) only, and we assume the eddies do not cross the equator.

100 The paper is organized as follows. The data and eddy detection methods used in this study are introduced in section  
101 2. Then GEM is introduced in section 3, including similarity vector, look-ahead approach and the worst-case  
102 runtime complexity i.e. computational complexity. Results including eddy tracks and examples of merging and  
103 splitting events in a sample area in the North Pacific are shown in section 4. The impacts of data noise and  
104 parameters uncertainties on the results are discussed in section 5. Finally, a summary and conclusions are given in  
105 section 6.

106

## 107 **2 Eddy identification**

### 108 **2.1 Input data**

109 The input data consists of the original altimetry field, which can come from satellite observations or numerical  
110 simulations. The altimetry field used in this study is the 20-year (1993-2012) daily SLA data from the merged and  
111 gridded satellite product of Maps of Sea Level Anomaly (MSLA) at  $0.25^\circ \times 0.25^\circ$  resolution in the global ocean  
112 from AVISO (<http://www.aviso.oceanobs.com/>). In this study, we use the “DT14” (delayed-time 2014) altimeter  
113 product [Duacs/AVISO, 2014], which is adequate for direct eddy detection [Capet et al., 2014] though it still has  
114 about 2-3 cm error globally for short temporal scales [Carrere et al., 2016]. A comprehensive discussion of gridded  
115 Aviso products for eddy investigations can be found in Chelton et al. (2011b).

116 We used the original SLA data (“DT14”) without any filtering or smoothing to identify eddies in this study.  
117 However, this does not imply that data smoothing is not needed for the SLA data in related studies (e.g. eddy  
118 dection, eddy tracking). For example, to calculate some eddy parameters (e.g., velocity and vorticity), smoothing  
119 may be required, as pointed out by Chelton et al. (2011b). Moreover, the data errors, even if they are very small,  
120 might affect to the eddy detection (see discussion in section 5.1).

### 121 **2.2 Eddy identification**

122 The eddy identification used in this study is similar to those used before [Chelton et al., 2011b; Mason et al., 2014],  
123 to identify eddies from SLA data. The eddies may be identified with multinuclear (two or more SLA extremes in  
124 one eddy) or mononuclear (only one SLA extremum in one eddy).The following mononuclear eddy definition is also  
125 similar to what was used by other authors [Chaigneau et al., 2011; Li et al., 2014; Li and Sun, 2015]. We have  
126 adopted the eddy detection step from Li and Sun (2015), which provides us with the necessary input for the tracking  
127 routines, namely eddy territories and boundaries. Each pixel has eight nearest neighbours. A point within the region  
128 is a local extremum if it has an SLA greater or less than all of its nearest neighbours. We also use such definition of  
129 extremum in our following analysis, in which the extrema are identified by checking each pixel in the map along

130 with the eight pixels around it. An eddy is defined as a simply-connected set of pixels that satisfies the following  
131 criteria:

132 (1) The SLA value of all of the pixels is above (below) a given SLA threshold;

133 (2) Only *one* SLA extremum exists in the pixel set;(3) The amplitude of the eddy (the max difference of SLA  
134 values) is larger than a critical value (e.g., 1 cm);

135 (4) The area of the eddy must be large enough for estimating eddy parameters (say >16 pixels).

136 Conditions (3)-(4) provide the lower bounds for eddy size and amplitude. These conditions automatically reduce the  
137 total number of detected eddies. Condition (1) is the same as the first criteria in Chelton et al., (2011b). It is used in  
138 consideration of the 2-3 cm of background SLA error [Carrere et al., 2016]; so, small fluctuations in SLA field  
139 would not be taken as eddies in this study. Condition (3) was generally used previously [Chaigneau et al., 2011;  
140 Chelton et al. 2011]. Condition (4) is more restrictive than the generally used value of eight pixels [e.g., Chelton et  
141 al., 2011; Li et al., 2014]; so, this condition is an add-on, which is potentially useful when deriving eddy parameters  
142 using a nonlinear optimal fitting method [Wang et al., 2015; Yi et al., 2015]. If the eddy area is too small (only a few  
143 pixels), its parameters (e.g. amplitude, area, radius, etc.) are very sensitive to its area (number of pixels). Besides, we  
144 don't put limits on eddy pixel number maximum (e.g., <1000) and eddy size (e.g., <400-1200 km) while such limits  
145 were generally used previously [e.g., Chelton et al. 2011; Mason et al., 2014].

146 The SLA extremum so determined is called eddy center. The set of pixels belonging to an individual eddy is referred  
147 to as the area of the eddy, and the outmost SLA contour is the boundary of the eddy. We use the area and boundary  
148 to calculate the similarity of eddies in section 3.2.

149 Each eddy is identified by the following procedures. First, according to condition (1), we find a simply-connected  
150 region with a given threshold of  $SLA > 3$  cm for cyclonic eddies and  $SLA < -3$  cm for anticyclonic eddies. Second, we  
151 check whether there is at least one extremum in the region. If the eddy is multinuclear, we use a segmentation  
152 method to segment them to satisfy condition (2). Finally, we check whether the region satisfies the eddy conditions  
153 (3) and (4), we remove those weak (amplitude < 1 cm) and small (pixels<16) eddies.

154

### 155 **2.3 Eddy segmentation for merging and splitting events**

156 Figure 2 illustrates the necessity for eddy segmentation based on the merging process of two eddies. Two different  
157 mononuclear algorithms are used in the upper and lower rows. In the top panels of Figure 2, eddies are identified by  
158 non-segmentation algorithm. Such mononuclear eddies may be very small. The time evolutions from  $t=1$  to  $t=3$   
159 show a decay scenario of two closed eddies C1 and C2. Both their amplitudes and areas become smaller and smaller  
160 with time. Then, a large eddy C3 suddenly appears in the same region without any premonition. It is hard to see  
161 what happened during the time from  $t=1$  to  $t=3$  from the parameters (amplitude and area) of mononuclear eddies  
162 identified by reducing the number of contours of the SLA until there is only one extreme in the contour (Chaigneau

163 et al., 2011) instead of the segmentation algorithm [Li and Sun, 2015]. In contrast, the bottom panels of Figure 2  
164 show a merging scenario of two closed eddies C1 and C2 using the segmentation algorithm [Li and Sun, 2015].  
165 During the time from  $t=1$  to  $t=2$ , both their amplitudes and areas are only marginally changed, while their distance is  
166 continually reduced. Then, a large eddy C3 naturally emerges in the same region, while C1 and C2 disappear. It is  
167 recognized from the eddy data that C3 is the merging result of C1 and C2.

168 Figure 3 illustrates this eddy segmentation strategy. Figure 3a shows two individual but nearby eddies. The pixels  
169 between the two dashed lines are naturally divided by the watershed (For basins, the “watershed” is a ridge between  
170 them, while it is a valley for plateaus). As shown in Fig. 3b, the cross section of the eddy clearly shows that two  
171 closely located pixels  $P_1$  and  $P_2$  on the left and right sides of watershed would slide along the path of steepest descent  
172 in the map of SLA data to different eddy centres. The shape of SLA can provide sufficient information to segment  
173 the multinuclear eddy into mononuclear ones.

174 Herein, we use the Mononuclear Eddy Identification (MEI) of the Universal Splitting Technology for Circulations  
175 (USTC) with watershed segmentation [Li and Sun, 2015] and include in our code the calculation of eddy  
176 parameters, including amplitude, radius, area, and boundary (Fig. 3), which might be potentially used in other  
177 studies [Sun et al., 2014].

178 The output eddy parameters from MEI is then used as input for our novel tracking algorithm GEM. The GEM  
179 mainly represents the logical relationship of eddies, which is less dependent on physical parameters which may  
180 change greatly because of dynamic evolution (e.g., splitting, merging). To this end, the GEM takes the previously  
181 identified eddies by MEI (with area/boundary, see section 2.2) as its input data.

182

### 183 **3 Dynamic tracking**

#### 184 **3.1 Overview of GEM**

185 The GEM is a logical model used for tracking the dynamic evolution of mesoscale eddies in the ocean (Fig. 4). The  
186 model essentially establishes logical relationships of previously identified eddies. The relationships are determined  
187 by two relatively independent steps i.e. the GEM algorithm consists of two parts (see Fig.4 for details): first,  
188 measuring the “map link” between two time steps and then connecting all time steps to the “track tree.”

189 The first part of GEM is “map link,” which uses as input eddy data obtained in the prior eddy identification step  
190 (area/boundary, see section 2.2) to establish the link of an eddy from one temporal snapshot to the next, namely  
191 living, missing, death, birth, and the associated dynamical processes of merging and splitting. In this part of the  
192 work flow, we use a 2-D vector rather than a passive scalar to measure the similarity between eddies  $E_1$  and  $E_2$  on  
193 two neighboring days (Figs. 5 and 6, see section 3.2.1 for details). We then use a relatively complex look-ahead  
194 procedure to solve the missing eddy problem (section 3.2.2). This new look-ahead approach has a duration of  $N$  days  
195 (Fig. 7). Finally, the links of the eddies in different snapshots are saved (see section 3.2.2 for details).

196 The second part is “track tree,” which uses the outputs from “map link” (i.e., eddy links), as its input (Fig. 4). It  
197 connects the eddy links from branches to a tree with the genealogical model (Fig. 8) using two sub procedures:  
198 “eddy branch” and “eddy tree.” In the “eddy branch” part, we use *parent* and *child* to define the eddy relationship  
199 and define all possible types of eddy states: birth, death, living, missing, merging and splitting (Fig. 8a).  
200 Consequently, we identify different roles in the eddy branches (see section 3.3.1 for details). Finally, in the “eddy  
201 tree” procedure, we connect the branches based on their roles (parent, child, and grandchild, etc.) in the genealogical  
202 tree (Fig. 8b). The output of GEM includes eddy tracks and the records of eddy relationships (see section 3.3.2 for  
203 details).

204 In short, the GEM uses previously identified eddies and/or their links to make dynamic tracks via a genealogical tree  
205 model. In addition to eddy territory and boundary, it needs two parameters as input, it includes two parameters, the  
206 critical value of area ratio  $r_c$  and  $N$ , as inputs. See section 5.2 for discussion on the impacts of these parameter  
207 choices.

## 208 3.2 Map link

209 To establish the relationships between the previously identified eddies, the first part of GEM used evaluates the  
210 similarity of these eddies which is defined here based on the overlap of the territory of an eddy in two consecutive  
211 time steps. It begins with defining similarity based on the overlapping area of eddies in consecutive time steps.  
212 Subsequently, the overlapping area which is closest to the one of the original eddy is defined to be the successor of  
213 the original eddy (if the threshold is met).

### 214 3.2.1 Eddy similarity

215 At first, the eddy similarity is calculated with an example (Fig 5a) before proceeding to the mathematical  
216 expressions. There were three eddies A1, A2 and B1 detected on March 28, 1997. In Figure 5b, there were four  
217 eddies, A1, A2, B1, and B2 on March 29, 1997. We overlapped the eddy territories into a single map (Fig. 5c). Then,  
218 we used the intersection of eddy territories on different days to calculate the similarity. For eddies A1 and A2, the  
219 intersections were very close to their respective territories on March 28 and 29. For eddy B1, the intersection was  
220 close to the area on the second day, but it was only part of that on the first day. Consequently, eddies A1 and A2 had  
221 full similarity on these days, while eddies B1 and B2 only had partial similarity on these days.

222 To estimate the above similarity, let us describe it in a mathematically logical way. As shown in Figure 6a, there is  
223 an eddy ( $E_1$ ) that is identified by the thick contour of Boundary 1 in the rectangular comparison region (not shown in  
224 figure) on day 0, and there are three eddies ( $E_2$ ,  $E_3$  and  $E_4$ ) that are identified in the same region on day 1. This  
225 comparison region, which is centered at the eddy center of  $E_1$ , moves in time with the target eddy ( $E_1$ ). To determine  
226 the similarities between  $E_1$  on day 0 and  $E_2$  to  $E_4$  on day 1, we intersect the territories of day 0 and day 1. For  
227 example, to determine the similarity between  $E_1$  and  $E_2$ , we count the overlap area  $S_{12}$  (defined as the intersection of  
228 Boundary 1 and Boundary 2) between  $E_1$  (area  $S_1$ ) and  $E_2$  (area  $S_2$ ), and then we calculate the following ratios:

229  $r_1 = S_{12} / S_1$  , (1a)

230  $r_2 = S_{12} / S_2$  . (1b)

231 Clearly, the values of  $r_1$  and  $r_2$  are within [0,1]. The larger  $r_1$  and  $r_2$  are, the larger possibility that  $E_2$  has to be the  
 232 snapshot of  $E_1$  on day 1. Eddy movement speeds are generally less than 0.1 m/s, which implies that an eddy can only  
 233 move one grid box(0.25°) in 3-4 days. Thus, the overlap on different subsequent days of the same eddy area should  
 234 be large enough. This is one of the parameters to set. When we applied GEM to track eddies in the Northern Pacific  
 235 Ocean, we choose  $r_c=2/3$ , and the choice of  $r_c$  is comprehensively addressed in section 5.2.

236 Using the vector  $(r_1, r_2)$  and the critical value  $r_c$ , we define four different types of similarity between two eddies (Fig.  
 237 6b). From low to high, they are as follows: Type 0 (T0), where  $E_1$  and  $E_2$  are unrelated; Type 1 (T1), where  $E_1$  on  
 238 day 0 is part of  $E_2$  on day 1 ( $E_1$  enlarging or merging); Type 2 (T2), where  $E_2$  on day 1 is part of  $E_1$  on day 0 ( $E_1$   
 239 decaying or splitting); and Type 3 (T3), where  $E_1$  and  $E_2$  are the same eddy at different locations on different days  
 240 ( $E_1$  living and moving). The last type (T3, living) is prescribed in cases when the center of  $E_1$  propagates less than a  
 241 pixel toward that of  $E_2$ , because the eddy movement speed is physically less than one grid (0.25°) per day. For  
 242 example, eddy B1 on March 29, 1997 in Figure 5b is simply assigned to T3 (living) even though  $r_1 < r_c$ . Eventually,  
 243 we obtain the relationships between  $E_1$  and  $E_3$  or  $E_4$  (Fig. 6a). Because the present method uses a vector to express  
 244 eddy similarity, we call it the similarity vector. This is an alternative to scalar similarity parameters [e.g., Ienna et al.,  
 245 2014; Mason et al., 2014].

246 For example, as shown in Figure 6a, the high similarity between  $E_1$  and  $E_2$  over a critical value  $r_c$  (marked as T3  
 247 (living) in Fig. 6b) suggests an evolution from  $E_1$  to  $E_2$ . This is similar for eddies  $E_1$  and  $E_3$ , but with a different  
 248 splitting relationship (marked as T2 (splitting) in Fig. 6b). The relationship between eddies  $E_1$  and  $E_4$  is designated  
 249 as “unrelated” because of the overlap in their territories is small or zero. In other words, their overlap rates are below  
 250 the critical value  $r_c$  (marked as T0 in Fig. 6).

251 In previous eddy tracking studies, simple methods were used for weekly SLA data (delayed-time 2010), e.g., the  
 252 closest distance between eddies [Chelton et al., 2011b; Yi et al., 2015], the closest angle between eddies [Zhang et  
 253 al., 2014] and the dimensionless similarity scalar [Chaigneau et al., 2008; Mason et al., 2014]. There is always a risk  
 254 of eddy jumping (from one track to another) in these methods, except for that of Pegliasco et al. (2015), who used  
 255 intersections of eddy boundaries to find the continuing eddy. Compared to the previous tracking methods, we use a  
 256 more robust technique to assess the relationship of eddies in subsequent time steps by using the overlap of their  
 257 territories. In addition, we do not simply assign the continuing eddy using the similarity vector for the two adjacent  
 258 days; rather, we try to solve the temporary missing eddy problem by looking ahead a few days.

### 259 3.2.2 Eddy Look-ahead

260 In contrast to the procedure used in Chelton et al. (2011b), we use a relatively complex look-ahead procedure. An  
 261 example for a given eddy are shown in Figure 7a. In the upper row, both  $Ec_1$  and  $Ec_2$  take the same eddy  $Ec_3$  as



262 their subsequent T1 type of eddy, which is a merging event (e.g., eddies C1 and C2 in Fig. 1). Since a T1 (merging)  
263 eddy has  $r_2 < r_c$  (intersection only takes a part of the eddy Ec3 on day 1), two or more eddies (e.g., Ec1 and Ec2) on  
264 day 0 could identify the same eddy (Ec3) as T1 eddy simultaneously on day 1. In the middle row, eddy E1 has two  
265 T2 (splitting) type of eddies (Ec2, Ec3) at the same time; this is a splitting event (e.g., eddies B1 and B2 in Fig. 5).  
266 In the lower row, eddy E1 has T2 (splitting) and T3 (living) types of eddies (respectively Ec2, Ec3) at the same time.  
267 Although there may be many possibilities for any given eddy, there is at most one eddy that can be marked as a T1  
268 (merging) or T3 (living) eddy on the following day (as  $r_l > r_c = 2/3$  holds).

269 This new look-ahead approach with  $N=2$  is shown in Figure 7b. After finishing the calculation of the following  
270 eddies on day 1, we continue to calculate eddies on the following days. At this preparation stage, it is similar to the  
271 MHA method with important modifications [Faghmous et al., 2013]. What makes this look-ahead procedure novel  
272 and efficient is that we use two simple rules to directly choose only one day's result for the following eddies. Thus,  
273 the procedure becomes linear without iteration, and it is much faster than the MHA, as discussed in the subsection  
274 on the computation complexity (section 3.6).

275 The two selection rules are: 1) the most similar first, and 2) the earliest day first. Rule 1 has priority. We first choose  
276 the most similar eddy as the potential successor of E1 according to their types. According to Figure 6b, T2 (splitting)  
277 type eddy covers only part of the original eddy while T1 (merging) eddy covers most part of the original eddy. The  
278 similarity from low to high is  $T2 < T1 < T3$ . For example, if there is only one T3 (living) eddy in these days, we  
279 choose it as the potential one. However, if there is more than one day with the same type of eddies, we need an  
280 additional rule: the earliest day first. For example, in the upper row of Figure 7b, there is one T3 (living) eddy on  
281 day 1, there is one T3 (living) eddy on day 2, and there are two T2 (splitting) eddies on day 3. In this case, we  
282 choose day 1 as the following day and the T3 (living) eddy as the following E1. In the middle and the lower rows,  
283 we choose day 2 and day 3 as the following days and the corresponding T3 (living) eddies as the following E1.

284

### 285 3.3 Track tree

#### 286 3.3.1 Eddy branch

287 After having determined the next subsequent days and the relationship types between eddies based on the above  
288 process, we can now establish the branches of an eddy from one day to the next. Eddy branch describes the  
289 relationship between two eddies at two different time steps. To describe the GEM more precisely, we use *parent* and  
290 *child* to identify the different roles that the eddy plays in eddy branches. There are three types of logical  
291 relationships used in GEM, as shown in Figure 8a.

292 The upper row shows a successor relationship: an eddy P on day 1 has only one successor (eddy P itself) on day 2.  
293 In this case, eddy P is allowed to be missing during day 1 and day 2. Additionally, eddy P will be recorded as death  
294 (black circle), if no successor eddy is found after  $N$  days.

295 In the middle row, two (or more) eddies merge into one. The first type includes principal and subordinate merging.  
 296 A principal eddy  $P_1$  and a subordinate eddy  $P_2$  on day 1 merge into a larger eddy  $P_1$  on day 2, whereas  $P_2$  is recorded  
 297 as death. This occurs when a large eddy meets and merges with a small eddy (e.g.,  $C_1$  and  $C_2$  in Fig. 1). The  
 298 anticyclonic eddies  $A_1$  and  $A_2$  in Fig. 11 also experience a similar process (see section 4.2 for details). The second  
 299 type is coordinated merging. Two (or more) parent eddies  $P_1$  and  $P_2$  merge to produce a new child eddy  $C$ , and all of  
 300 the parent eddies are recorded as death. This is because the similarity was not sufficiently high for either eddy to  
 301 which the record of eddy  $C$  should be appended. There might be another choice by keeping parent eddies  $P_1$  and  $P_2$   
 302 alive and appending the record of eddy  $C$  to both eddies. This choice artificially increases lifetimes of eddy  $P_1$  and  
 303  $P_2$  and leads to other tracking problems; so, we abandon it.

304 In the lower row, a parent eddy splits into several child eddies. The first type is principal and subordinate splitting. A  
 305 parent eddy  $P$  splits into an eddy  $P$  (itself) and a child eddy  $C$ , which is recorded as birth. The second type is  
 306 coordinated splitting. Two (or more) child eddies are born from the parent eddy  $P$ , which is then recorded as death.

### 307 3.3.2 Eddy tree

308 Finally, the track tree is recorded by connecting the eddy branches (Fig. 8b). Track tree of an eddy records  
 309 information of all the associated eddies (e.g., living, death, birth, merging and splitting, etc.) during its entire life. In  
 310 this process, the role that an eddy plays in the track tree is considered. The first generation is the parent eddy (e.g.,  
 311  $P_1$ ), the second generation is the child eddy (e.g.,  $C_1$ ) and the third generation is the grandchild eddy (e.g.,  $G_1$ ). The  
 312 track tree uses the above eddy branches (Fig. 8a). We connect the branches from one time to another to obtain the  
 313 whole eddy track tree.

314 There are two additional notations. First, an eddy emerging from the same family of eddies (e.g., two siblings  $C_2$  and  
 315  $C_4$ ) will be recorded as a new family member (e.g., eddy  $C_5$ ). Second, an eddy merging from two different families  
 316 of eddies (e.g.,  $C_1$  and  $P_2$ ) will be recorded as a new eddy  $N_1$ .

317 Although the model could have several generations, we only recorded two generations i.e. parent and child in this  
 318 study due to the complexity of the output data structure and the computational complexity. However, we can  
 319 indirectly track other generations using the relationships between them.

## 320 3.4 Computation complexity

321 To calculate similarity vectors, we need to overlap two small regions around eddy  $E_1$ . The total number of pixels in  
 322 the rectangular comparison region is  $L$ . The computational complexity of the similarity vector is  $O(L)$  for each day.  
 323 If we use  $N$  look-ahead time steps to find the best choice, the computation complexity of the branches will be  $O$   
 324  $(L(N+1))$  for one eddy. Because all of the steps are linear without iteration, given the maximum number of eddies in  
 325 any time frame  $M$ , the number of look-ahead time steps  $N$  and the total number of time steps  $T$ , the total computation  
 326 complexity is  $O(LM(N+1)T)$ . The GEM algorithm can hardly be made any faster. When the number of look-ahead  
 327 time steps  $N$  is more than one, the computation complexity is much faster than  $O(M^{N+1}T)$  of MHA.

328 For example, both  $L$  and  $M$  are approximately 1000, and  $N=2$  is used in the present study. The MHA method will  
329 require on the order of  $10^2$ - $10^3$  times more computational time than the present method; and the larger the value of  $N$ ,  
330 the more efficient the present method is. The look-ahead time  $N$  may be potentially as large as one week ( $N=6$ ), as  
331 noted in the following discussion. Thus, the present method is especially effective compared to the previously  
332 suggested methods when a long look-ahead time is required for poorly identified eddies.

333

## 334 4 Results

### 335 4.1 Eddy tracks

336 We first apply the MEI to detect the ocean eddies in the North Pacific Ocean (NPO) during 1993-2012. The eddy  
337 centers (SLA extrema of eddy snapshots) on each day are counted on each  $1^\circ \times 1^\circ$  grid. In general, anticyclonic eddies  
338 are significantly more frequent than cyclonic eddies. As shown in Figure 9a, the cyclonic eddies are mainly located  
339 in the western part of the NPO. For example, there are lots of cyclonic eddies east of Japan near the Kuroshio, which  
340 can also be seen from both Figure 1 and the results in section 5.1. In contrast, anticyclonic eddies are mainly located  
341 in the eastern part of the NPO (Fig. 9b). For example, the eddies are mainly anticyclones in the red box, which can  
342 also be seen from the results in section 4.2. In general, the eddies are ubiquitous in Figure 9c (about 50-70 eddies per  
343 year on each  $1^\circ \times 1^\circ$  grid), except that there are several regions where both types of eddies are relatively scarce. One  
344 of them is known as “eddy desert” (black box in Figure 9c) [Chelton et al., 2007]. The other region is the North  
345 Equatorial Current (NEC) (blue box in Figure 9c) [Hu et al., 2015]. Finally, we present in Figure 9d the ratio of  
346 difference of the numbers of cyclonic and anticyclonic eddies to the total number of eddies.

347 We apply the GEM to these eddies detected by MEI with  $r_c=2/3$  and  $N=2$ . In the NPO, there are a total of 60276  
348 eddies with lifetimes longer than 30 days. Among them, 37553 of the eddies are anticyclonic and 22723 are cyclonic.  
349 The tracks of long-lived eddies are plotted in Figure 10. In general, they are similar to those shown in previous  
350 studies [Chelton et al., 2011b]. There are 7290 anticyclonic and 3627 cyclonic eddies with lifetimes longer than 100  
351 days (Fig. 10a), and the ratio of anticyclonic to cyclonic eddies is approximately 2. The ratio is larger for eddy  
352 lifetimes greater than 400 days, which was also noted in previous studies [Chelton et al., 2011b; Xu et al., 2011].  
353 Each track is very smooth because we require that the snapshots of eddies on different days overlap one another. We  
354 have done a visual evaluation of many long-lifetime eddy trajectories and the quality of the tracking results is  
355 reasonable. We will take the long-lived C1 in Figure 10b as an example.

356 Eddy C1 was first detected as an eddy initiated on September 14, 1995, with an extremum at  $163.5^\circ\text{W}$ ,  $10.5^\circ\text{N}$ . It  
357 then travelled to the northwest and disappeared at  $151.25^\circ\text{W}$ ,  $20.5^\circ\text{N}$  on March 11, 1997. Its trajectory is the longest  
358 that we have detected in the NPO (Fig. 10b). The trajectory is smooth, except for a sudden jump from  $167.5^\circ\text{E}$  to  
359  $166.75^\circ\text{E}$  (Fig. 10c) on July 31, 1996. The GEM algorithm did very well at whether we should connect the  
360 trajectories from before July 30, 1996 with that after July 31, 1996, into a single trajectory.

361 To clarify this, we plot the two SLA fields in Figure 10d. The SLA field on July 30, 1996 is plotted as contours. The  
362 eddy center is marked by a black cross at 167.5°E, 16.5°N. In contrast, the SLA field on July 31, 1996 is plotted in  
363 shading. The eddy center is marked by a red cross at 166.75°E, 17.25°N. The distance between the eddy extrema was  
364 larger than 100 km within a day. Although that distance is far beyond the criterion applied in standard eddy tracking  
365 routines [Mason et al., 2014; Yi et al., 2015], we can see from the SLA fields that they both indicated the same eddy,  
366 and that it was consistent with our approach to connect the trajectories into a single trajectory.

367 There may be no associated eddy can be identified at the next time step for an eddy at time step  $k$ , and it may be the  
368 result of eddies temporarily “disappearing” for a variety of reasons related to sampling errors and measurement  
369 noise [Chelton et al., 2011b]. The application of similarity vector and look-ahead procedure can effectively  
370 accommodate such problems and allow for the reappearance of temporarily “disappearing” eddy in the tracking  
371 procedure. In turn, it reduces the usage of the look-ahead procedure. It is clear that the similarity expressed as a  
372 vector is better than that as scalar using simple distance.

## 373 4.2 Eddy merging and splitting

374 The trajectories provide evidence of dynamic evolution. The time evolution of a couple of anticyclonic eddies is  
375 depicted in Figure 11a, which implies a merging process occurring in the red boxes in Fig. 9. As shown in Figure  
376 11a, eddy A1 had a westward movement with a speed of 2.6 cm/s, and eddy A2 lingered near 133°W. Then, both  
377 eddies merged into one large eddy on April 23, 1997. That evolutionary process is clearly shown by the SLA fields  
378 (Figs. 11c-j). In Figure 11c, there were two anticyclonic eddies, A1 and A2, located at 132°W, 28.5°N. Eddy A1  
379 moved from east to west with a nearly constant speed of 2.6 cm/s, whereas eddy A2 had negligible zonal motion.  
380 They then rotated clockwise about each other with an average angular velocity of  $6 \times 10^{-7} \text{ s}^{-1}$ , as denoted by the blue  
381 arrows. Finally, they merged into the new large eddy A2 (see animation in supplement).

382 The SLA field shows that an eddy splitting process also occurred in the box the same time. The time evolutions of  
383 anticyclonic eddies B1, B2 and B3 are depicted in Figure 11b. At first, eddy B1 had a fast westward speed of 10.4  
384 cm/s. It then split into two eddies (B1 and B2) on March 29, 1997 (Fig. 6). Eddy B1 traveled at its original speed  
385 whereas eddy B2 lingered at its origin. Then, eddy B3 emerged at a location between B1 and B2 on April 9, 1997,  
386 which slowed down the speed of B1 to approximately 3.5 cm/s. After that, eddies B2 and B3 merged into a new  
387 eddy B3 on April 19, 1997. In fact, similar to eddies A1 and A2, eddies B1 and B2 eventually merged into a new  
388 eddy on May 20, 1997 (not shown). The SLA maps in Figures 11c-j show more details that were not recorded by the  
389 eddy tracking data. Note that eddy B2 had a very short lifetime of 20 days but a complex dynamic process. If only  
390 long-term eddies (lifetime > 30 days) were saved, the corresponding evolutionary process might not be recorded  
391 properly.

392 It is expected that a pair of cyclonic eddies will have a counter-clockwise rotation in the Northern Hemisphere,  
393 which is known as the Fujiwhara effect for atmospheric cyclones [Fujiwhara, 1921]. When two cyclones are close  
394 enough, they will begin to orbit cyclonically (counter-clockwise in the Northern Hemisphere). Because the above-

395 mentioned eddies are anticyclonic, they have opposing directions of rotation, which appear as two point vortices  
396 moving in circular paths about the center of vorticity in classical fluid dynamics [Batchelor, 1967].

### 397 **4.3 Census of merging and splitting events**

398 To illuminate how often the merging and splitting processes occurred, we counted the total number of merging and  
399 splitting events on each  $1^\circ \times 1^\circ$  grid each year. The merging and splitting events were homogeneously distributed in  
400 the oceans, but in general were very few times each year per  $1^\circ \times 1^\circ$  grid element. The merging frequencies for  
401 cyclonic eddies and anticyclonic eddies are shown in Figure 12, which are similar to their splitting frequencies (not  
402 shown). The distribution pattern of merging frequencies for cyclonic eddies in Figure 12a, is very similar to that of  
403 cyclonic eddy centers in Figure 9a. In contrast, the merging frequency for anticyclonic eddies was larger along the  
404 west coast (Fig. 12b), whereas the anticyclonic eddy centers were located mainly in the east (Fig. 9b). Although  
405 merging and splitting events may occur anywhere in the ocean there is spatial variation in the number of events (Fig  
406 12c, d)..

407 The first type of special region is the western boundary. It is known that the western boundary is a sink of eddy  
408 energy caused by the interaction with the bottom and lateral topography [Zhai et al., 2010]. It is also known as a  
409 “graveyard” for westward-propagating ocean eddies [Zhai et al., 2010; Chelton et al., 2011b]. The second type of  
410 special region is located in strong currents, including the Kuroshio Current, and the NEC [Hu et al., 2015]. Among  
411 those currents, the eddies in the NEC had the highest frequency of merging and splitting events, which was not  
412 noted in previous studies. The third type of special region is located in the northeast Pacific, which is also known as  
413 an “eddy desert” [Chelton et al., 2007]. The fourth type of special region is located in enclosed marginal seas,  
414 especially the Bering Sea.

415 By comparing Figure 12 with Figure 10, we can see that the regions with high frequencies of merging and splitting  
416 events have relatively few eddy tracks, especially in the NEC (blue box in Figure 9c) and in the “eddy desert” (black  
417 box in Figure 9c) in the northeast Pacific. The existence of “eddy desert” may be due to the fact that the eddy was  
418 too small to be detected or the fact that the eddy lifetime was too short [Chelton et al., 2011b]. However, Figures 9  
419 and 12 suggest that merging and splitting events may be a major contributor to the “eddy desert”.

420 We also calculate the average dynamic (merging and splitting) events per eddy as a function of lifetime (Figure 13).  
421 The results are similar regardless eddy polarizations and dynamic types. The merging and splitting events are  
422 approximately linear increase with eddy lifetime. However, the anticyclonic eddies seem more vigorous in ocean  
423 dynamics than cyclonic eddies.

424

## 425 5 Discussion

### 426 5.1 Data noises

427 Although “the Aviso product DT14” is much better than previous products, there are still some notable errors,  
428 especially for short temporal scales of less than two months [Carrere et al., 2016]. It was reported that there are  
429 along-track SLA errors of about 2-3 cm globally and of more than 3 cm at high latitudes and in shallow waters.

430 To reduce the noises in SLA data, one may use the Gaussian structure filter [Chelton et al., 2011b; Mason et al.,  
431 2014], Hanning filters [Penven et al., 2005], or Lanczos filter [Chaigneau et al., 2008]. As certain parameters need to  
432 be chosen in these filters, the filtered results depend much on these parameters [see Fig. A1 in Chelton et al., 2011b].  
433 As sensitivity test we apply a simple five-point quadratic smoothing to the SLA data. The filtered data are then  
434 piecewise  $C^2$ -smoothed by a quadratic function, which satisfies the potential requirements for calculating vorticity  
435 (second derivative of SLA) from SLA data.

436 Figure 14 shows the non-smoothed and smoothed SLA data from January 1, 1993 to January 4, 1993. The smoothed  
437 SLA maps are very close to the non-smoothed SLA maps. And the values at the SLA extrema (not shown) are close  
438 to their original values. This implies that the noise in the DT14 data is sufficiently small for our purpose.

439 However, the noises cannot be neglected, even when they are small. They might induce additional SLA extrema (see  
440 the definition of extremum in section 2.2), which eventually affect eddy detection, e.g., the additional extremum on  
441 January 2, 1993 in box A and the additional extremum on January 3, 1993 in box B (Figure 14). These additional  
442 extrema existed only for a very short period (one or two days). But they can induce additional merging and splitting  
443 events, which may cause eddies to unexpectedly terminate [Chelton et al., 2011b]. The ambiguity of the eddy  
444 identification procedure, which may be caused by sampling errors and measurement noise in the input SLA data,  
445 strongly suggest the application of a look-ahead approach.

### 446 5.2 Impact of variations of parameters

447 To discuss the impact of parameters  $N$  and  $r_c$ , we carry out a sensitivity study in the north Pacific from year 1993 to  
448 2012. There are two parameters in the GEM: the critical value  $r_c$  and the look-ahead time  $N$ . The number of eddies  
449 with lifetimes  $> 30$  days is counted for different  $r_c$  and  $N$ , as shown in Figure 15a. Note that the results are very  
450 similar, except for  $N=0$  (i.e., without any look-ahead). It is from the above discussion that we see look-ahead is  
451 necessary when there are extrema due to small noises in the data. The number of eddies does not change  
452 substantially with  $r_c$  for any  $N>1$ , when  $r_c$  is within 0.5 to 0.8 (e.g. 63469 eddies were identified with  $N=2$ ,  $r_c=0.5$   
453 and the identified eddies number was 63630 with  $N=4$ ,  $r_c=0.8$ . Meanwhile, the numbers of merging and splitting  
454 events are also counted for different  $r_c$  and  $N$ , as shown in Figure 15b. In general, the splitting events occurs slightly  
455 more frequently than the merging events (e.g. 151220 splitting events and 150612 merging events for  $N=2$ ,  $r_c=0.5$ ).  
456 Note also that the results are very similar, except for  $N=0$ . The numbers of merging and splitting events seem to  
457 converge for  $r_c > 0.5$  as  $N$  increases. For each  $N>0$ , the numbers of merging and splitting events reach a maximum at

458  $r_c=0.6$ . A relatively loose similarity condition ( $r_c<0.5$ ) will lead to a risk of eddy jumping from one track to another,  
459 which consequently reduces both total eddy number and dynamic events. On the other hand, a relatively strict  
460 similarity condition ( $r_c>0.9$ ) will lead to a risk of missing eddies, which may also reduce both total eddy numbers  
461 and dynamic events.

462 In general, one would like the tracking results to be insensitive to the choice of these parameters. From Figure 15,  
463 we can observe that  $0.5<r_c<0.8$  appears to be a choice with relatively robust results. The optimal value for  $r_c$  might  
464 be 0.6-0.7, which is reasonable. In one hand, we first require that  $r_c >0.5$ . On the other hand, we know there is area  
465 error in calculation ( $\sim 10\%$ ) since only eddy grids are taken into consider. This is also the reason why we need  $r_c$   
466  $<0.9$  or even smaller. So the optimal value should be within 0.5-0.9, and  $\sim 0.7$  is just in this middle. We also find that  
467 the look-ahead time  $N$  should be larger than 0; otherwise, the risks of eddy jumping and eddy missing are too great.  
468 The look-ahead approach effectively reduces such risks. For example,  $N=1$  and  $N=2$  have 95.5% and 98% of the  
469 total eddies for  $N=4$ , respectively. To reduce the missing eddies to 1%, the look-ahead time might be greater than six  
470 days. This is also the physical requirement of the representative period of the merged SLA data [Chelton et al.,  
471 2011b]. Although  $N=4$  might be better,  $N=2$  produced a very similar result ( $\sim 2\%$  bias to  $N=4$ ) and with a  
472 significantly lower computational cost. Our present parameters are reasonable considering of computational cost.

473 It should be pointed out that GEM is relatively independent to MEI, but the ratios  $r_1$ ,  $r_2$  and  $r_c$  might be sensitive to  
474 the method used in identification. We noted that O-W based identification is much sensitive than SLA based one,  
475 since O-W based eddies are much smaller and more possible to be unreal [Chaigneau et al., 2008]. Besides,  $r_c$  may  
476 not be independent with  $N$ , and the present  $r_c$  should only be valid for small time steps. If the time step is too large,  
477 the distance of eddy motion may be too far. And eddy snapshots can't overlap with each other. This constrain for  
478 time step is something like the Courant–Friedrichs–Lewy (CFL) condition (for time step) in computer fluid  
479 dynamics. In general, we think any tracking method should have this time-step limitation (depending on eddy  
480 size/propagation speed), if one don't want to mix one signal with another.

481 Finally, as noted in section 4.2, there are short-term eddies (lifetime  $< 30$  days), which might to though complex  
482 evolution process. If only long-term eddies (lifetime  $> 30$  days) were saved, the corresponding evolution process  
483 might not be recorded properly. This should be noted in further applications on eddy dynamics with satellite  
484 altimetry data.

### 485 **5.3 Impact of eddy boundary**

486 It is difficult to directly compare the influences of eddy boundary due to parameter choice in eddy identification. We  
487 can, however, estimate the influence of the eddy boundary using an indirect way. Because the eddy center is  
488 relatively robust, different identification methods mainly give different eddy boundaries. Consequently, the eddy  
489 area  $S$  is most sensitive to such an eddy area. However, the area ratio reduces the sensitivity to the eddy area  $S$   
490 because both the overlap area  $S_{I2}$  and the eddy area  $S$  change synchronously. Moreover, our tracking results  
491 fortunately are not very sensitive to  $r_c$  (or the eddy area  $S$ ), as noted in the above discussion. For example, the

492 present results are based on a very strict identification method. If we modify the threshold of eddy amplitude from 1  
493 cm to 3 cm, the number of identified eddies will decline. Nevertheless, the identification results for the long-lived  
494 eddies appear to be similar (Table 1).

495 However, such sensitive test may be only valid for the comparison of different parameter values in a same  
496 identification method. It can't be simply extended to the comparison of varies identified eddies by different  
497 identifications, since the eddy detection algorithms distinguish a lot with each other. In general, the automated eddy  
498 detection algorithms are categorized into three types: 1) physical parameter-based algorithms, e.g., Okubo–Weiss  
499 (O–W) parameter [Isern-Fontanet et al., 2003; Chaigneau et al., 2008]; 2) flow geometry-based algorithms  
500 [Chaigneau et al., 2011; Chelton et al., 2011b; Wang et al., 2015]; and 3) hybrid methods, which involve physical  
501 parameters and flow geometry characteristics [Nencioli et al., 2010; Xiu et al., 2010; Dong et al., 2011; Yi et al.,  
502 2015]. For example, Yi et al. (2015) used the O–W parameter to identify eddy kernels and SLA contour geometries  
503 to identify eddy boundaries. So it is difficult to compare the influences of eddy territory by using different  
504 identification and tracking algorithms.

505

#### 506 **5.4 Future research**

507 The GEM is a flexible model that can easily work with other relevant programs, e.g., data filtering and smoothing  
508 algorithms [Chelton et al., 2011b; Ienna et al., 2014; Wang et al., 2014], other hybrid eddy detection algorithms [e.g.,  
509 Yi et al., 2015] and O-W parameter detection [e.g., Petersen et al., 2013], because the GEM only requires a flow  
510 field and previously identified eddies to accomplish dynamic tracking. In addition, the similarity measurement can  
511 be replaced by similar methods [e.g., Pegliasco et al., 2015] when considering more complex conditions.

512 The identified eddies by using other identification algorithm without watershed can also be tracked with the GEM.  
513 In this case, the strong interaction stage of eddies “in conjunction”, which leads to genesis and termination of eddies,  
514 is more likely missed as pointed out in section 2.3. However, the weak interaction stage of eddies (watershed free) in  
515 some far distance could still be recorded, because most of merging/splitting records occurred at the interaction of  
516 two eddies with a certain distance. This weak interaction still can't be recorded by previously interaction-free  
517 tracking algorithm, which records only the isolated tracks. Thus the GEM extends the potential applications of  
518 previously identified eddies.

519 The GEM is a complex model. The output data include eddy tracks, relationships and previously identified eddy  
520 characteristics (e.g., amplitude and radius). These eddy characteristics, which were directly obtained from the  
521 identification process, are useful for censuses [Chelton et al., 2011b]. However, they may not be sufficiently  
522 accurate for some applications. For example, eddy area was required in our recent studies on typhoons and oceanic  
523 eddy interactions [Sun et al., 2010, 2012, 2014]. Besides, some physical quantity (circulation, angular momentum,  
524 energy) are required to be accurately calculated in the investigation of eddy dynamics process. A better way to



525 obtain these characteristics might be to use a nonlinear fitting of the flow field [Wang et al., 2015; Yi et al., 2015]  
526 with appropriate models [e.g., Sun, 2011; Zhang et al., 2013] other than simply estimated from identification.

527 Another future research direction may involve comparing different tracking datasets. Because there are several  
528 tracking datasets produced by various methods, it is useful to inter-compare them. This may improve both the  
529 tracking methods and the available datasets for further studies.

530 The GEM can be easily applied to larger datasets, even to 3-D numerical simulation outputs [Petersen et al., 2013;  
531 Woodring et al., 2016], because its computational time increases only linearly as a function of the size of the dataset.  
532 The computation of the 20-year daily global SLA data only required a few hours on a personal computer. In a  
533 personal computer with CPU of i7-6700k and 4.00 GHz, it takes about 15 minutes to identify snapshots of eddies,  
534 about 20 minutes to establish similarity, and about 10 minutes to track eddies in the North Pacific Ocean (NPO) with  
535  $0.25^\circ \times 0.25^\circ$  resolution of 20-year daily “DT14” data. Such a model can be used to analyze numerical simulation  
536 outputs.

537 The GEM opens a window to investigate eddy dynamics [Wang et al., 2015] and other applications [Sun et al., 2014]  
538 on those problems, e.g. (i) the strong eddy interaction which leads to genesis and termination of eddies (ii) the weak  
539 eddy interaction which associates with merging/splitting events (iii) the weak eddy interaction which modulates the  
540 eddy track and motion. As illuminated in Figure 11, the dynamic evolution of eddies is accompanied by abundant  
541 phenomena that might be identified using the GEM. The present study is only the beginning of such applications.

542

## 543 **6 Conclusions**

544 We have introduced the GEM for the tracking of the dynamic evolution of mesoscale eddies in the ocean. Several  
545 novel approaches (e.g., vector similarity and look-ahead approach) were applied to deal with unsolved problems in  
546 tracking. All of the computational steps in GEM are linear and do not require iteration. Given the grid number of the  
547 target region  $L$ , the maximum number of eddies  $M$ , the number of look-ahead time steps  $N$ , and the total time steps  $T$ ,  
548 the total computational complexity is of  $O(LM(N+1)T)$ . We applied the GEM to the eddies in the north Pacific.  
549 Eddy tracks were smooth because we required that the snapshots of eddies on neighboring days overlap one another.  
550 Both merging and splitting rates of eddies were high, especially at the western boundary, in strong currents and in  
551 “eddy deserts.” The GEM is useful not only for satellite-based observational data but also for the output of  
552 numerical simulations. It potentially has many applications for studies of dynamic processes in related fields, e.g.,  
553 the dynamics of cyclones in meteorology. The “MEI” and “GEM” computer codes and program manual will be  
554 provided openly at the website [https://www.researchgate.net/profile/Liang\\_Sun20/](https://www.researchgate.net/profile/Liang_Sun20/) after publication of this  
555 paper.

556

557

558 **Acknowledgements**

559 We thank the anonymous referees for their comments and suggestions. We thank the AVISO for providing the SLA  
560 data (<http://www.aviso.oceanobs.com/>). This work was supported by the National Basic Research Program of China  
561 (Nos. 2012CB417402 and 2013CB430303), the National Foundation of Natural Science (No. 41376017) and the  
562 Open Fund of the State Key Laboratory of Satellite Ocean Environment Dynamics (No. SOED1501).  
563

564 **References**

- 565 Batchelor, G. K. (2000). *An introduction to fluid dynamics*. Cambridge university press, 615pp.
- 566 Bennett, A. F., & White, W. B. (1986). Eddy heat flux in the subtropical North Pacific. *J. Phys. Oceanogr.*, 16(4),  
567 728-740.
- 568 Capet, A., E. Mason, V. Rossi, C. Troupin, Y. Faugère, I. Pujol, and A. Pascual, (2014), Implications of refined  
569 altimetry on estimates of mesoscale activity and eddy-driven offshore transport in the Eastern Boundary Upwelling  
570 Systems, *Geophys. Res. Lett.*, 41, 7602–7610, doi:10.1002/2014GL061770.
- 571 Carrere, L., Faugère, Y., and Ablain, M. (2016). Major improvement of altimetry sea level estimations using  
572 pressure-derived corrections based on ERA-Interim atmospheric reanalysis, *Ocean Sci.*, 12, 825-842,  
573 doi:10.5194/os-12-825-2016.
- 574 Chaigneau, A., Gizolme, A., and Grados, C. (2008). Mesoscale eddies off Peru in altimeter records: identification  
575 algorithms and eddy spatio-temporal patterns. *Progr. Oceanogr.*, 79, 106–119.
- 576 Chaigneau, A., Le Texier, M., Eldin, G., Grados, C., and Pizarro, O. (2011). Vertical structure of mesoscale eddies  
577 in the eastern South Pacific Ocean: A composite analysis from altimetry and Argo profiling floats, *J. Geophys. Res.:  
578 Oceans*, 116. C11025, doi:10.1029/2011JC007134.
- 579 Chelton, D.B., Schlax, M.G. (1996). Global observations of oceanic Rossby waves. *Science* 272, 234–238.
- 580 Chelton, D. B., Schlax, M. G., Samelson, R. M., & de Szoeke, R. A. (2007). Global observations of large oceanic  
581 eddies. *Geophys. Res. Lett.*, 34(15), L15606,. doi:10.1029/2007GL030812.
- 582 Chelton, D. B., Gaube, P., Schlax, M. G., Early, J. J., & Samelson, R. M. (2011a). The influence of nonlinear  
583 mesoscale eddies on near-surface oceanic chlorophyll. *Science*, 334(6054), 328-332.
- 584 Chelton, D. B., Schlax, M. G., & Samelson, R. M. (2011b). Global observations of nonlinear mesoscale eddies.  
585 *Progr. Oceanogr.*, 91(2), 167-216.
- 586 Dong, C., Nencioli, F., Liu, Y., & McWilliams, J. C. (2011). An automated approach to detect oceanic eddies from  
587 satellite remotely sensed sea surface temperature data. *Geoscience and Remote Sensing Letters, IEEE*, 8(6), 1055-  
588 1059.
- 589 Dong, C., McWilliams, J. C., Liu, Y., & Chen, D. (2014). Global heat and salt transports by eddy movement. *Nature  
590 communications*, 5:3294, DOI: 10.1038/ncomms4294.
- 591 Duacs/AVISO (2014), A new version of SSALTO/Duacs products available in April 2014. Version 1.1, CNES.  
592 [Available at [http://www.aviso.altimetry.fr/fileadmin/documents/data/duacs/](http://www.aviso.altimetry.fr/fileadmin/documents/data/duacs/Duacs2014.pdf) Duacs2014.pdf].
- 593 Fang, F., and Morrow, R. (2003). Evolution, movement and decay of warm-core Leeuwin Current eddies. *Deep-Sea  
594 Res., Part II* 50, 2245–2261.

595 Fujiwhara, S. (1921). "The natural tendency towards symmetry of motion and its application as a principle in  
596 meteorology". *Q. J. R. Met. S.* 47 (200): 287–293. doi:10.1002/qj.49704720010.

597 Faghmous, J. H., Uluyol, M., Styles, L., Le, M., Mithal, V., Boriah, S., & Kumar, V. (2013). Multiple Hypothesis  
598 Object Tracking For Unsupervised Self-Learning: An Ocean Eddy Tracking Application. In *AAAI*.

599 Hu, D., Wu, L., Cai, W., Gupta, A. S., Ganachaud, A., Qiu, B., ... & Wang, G. (2015). Pacific western boundary  
600 currents and their roles in climate. *Nature*, 522(7556), 299-308.

601 Ienna, F., Jo, Y. H., & Yan, X. H. (2014). A new method for tracking Meddies by satellite altimetry. *Journal of*  
602 *Atmospheric and Oceanic Technology*, 31(6), 1434-1445.

603 Isern-Fontanet, J., García-Ladona, E., & Font, J. (2003). Identification of marine eddies from altimetric maps.  
604 *Journal of Atmospheric and Oceanic Technology*, 20(5), 772-778.

605 Li, Q. Y., Sun, L., Liu, S. S., Xian, T., & Yan, Y. F. (2014). A new mononuclear eddy identification method with  
606 simple splitting strategies. *Remote Sensing Letters*, 5(1), 65-72. doi:10.1080/2150704X.2013.872814.

607 Li, Q. Y., & Sun, L. (2015). Technical Note: Watershed strategy for oceanic mesoscale eddy splitting. *Ocean*  
608 *Science*, 11(2), 269-273. doi: 10.5194/os-11-269-2015.

609 Mason, E., Pascual, A., & McWilliams, J. C. (2014). A new sea surface height–based code for oceanic mesoscale  
610 eddy tracking. *Journal of Atmospheric and Oceanic Technology*, 31(5), 1181-1188.

611 McGillicuddy, D. J. (2011). Eddies masquerade as planetary waves. *science*, 334(6054), 318-319. doi:  
612 10.1126/science.1208892.

613 Nencioli, F., Dong, C., Dickey, T., Washburn, L., & McWilliams, J. C. (2010). A vector geometry-based eddy  
614 detection algorithm and its application to a high-resolution numerical model product and high-frequency radar  
615 surface velocities in the Southern California Bight. *Journal of Atmospheric and Oceanic Technology*, 27(3), 564-579.

616 Penven, P., Echevin, V., Pasapera, J., Colas, F., and Tam, J.: Average circulation, seasonal cycle, and mesoscale  
617 dynamics of the Peru Current System: A modeling approach, *J. Geophys. Res.*, 110, C10021,  
618 doi:10.1029/2005jc002945, 2005.

619 Petersen, M. R., Williams, S. J., Maltrud, M. E., Hecht, M. W., & Hamann, B. (2013). A three-dimensional eddy  
620 census of a high-resolution global ocean simulation. *Journal of Geophysical Research: Oceans*, 118(4), 1759-1774.

621 Pegliasco, C., A. Chaigneau, and R. Morrow, (2015). Main eddy vertical structures observed in the four major  
622 Eastern Boundary Upwelling Systems, *J. Geophys. Res. Oceans*, 120, 6008–6033, doi:10.1002/2015JC010950.

623 Sun L, Yang Y.-J., Xian T., Lu Z. and Fu Y.-F., (2010). Strong enhancement of chlorophyll a concentration by a  
624 weak typhoon, *Mar. Ecol. Prog. Ser.*, 404, 39-50, doi: 10.3354/meps08477.

625 Sun, L. (2011). A typhoon-like vortex solution of incompressible 3D inviscid flow. *Theoretical and Applied*  
626 *Mechanics Letters*, 1(4), 042003.

627 Sun, L., Yang, Y.-J., Xian, T., Wang, Y., and Fu, Y.-F., (2012). Ocean responses to Typhoon Namtheun explored  
628 with Argo floats and multiplatform satellites. *Atmos. Ocean.* 50(sup1), 15-26.

629 Sun, L., Y.-X. Li, Y.-J. Yang, Q. Wu, X.-T. Chen, Q.-Y. Li, Y.-B. Li, & T. Xian (2014). Effects of super typhoons  
630 on cyclonic ocean eddies in the western North Pacific: A satellite data-based evaluation between 2000 and 2008, *J.*  
631 *Geophys. Res. Oceans*, 119(9): 5585–5598, doi:10.1002/2013JC009575.

632 Wang, R., Yang, Z., Liu, L., Deng, J., & Chen, F. (2014). Decoupling noise and features via weighted L1-analysis  
633 compressed sensing. *ACM Transactions on Graphics (TOG)*, 33(2),1-12.

634 Wang, Z., Li, Q., Sun, L., Li, S., Yang, Y., & Liu, S. (2015). The most typical shape of oceanic mesoscale eddies  
635 from global satellite sea level observations. *Frontiers of Earth Science*, 9(2), 202-208. doi: 10.1007/s11707-014-  
636 0478-z.

637 Woodring, J., Petersen, M., Schmeiber A., Patchett J., Ahrens J., Hagen H., (2016). In Situ Eddy Analysis in a High-  
638 Resolution Ocean Climate Model, *IEEE Transactions on Visualization & Computer Graphics*, 22(1), 857-866,  
639 doi:10.1109/TVCG.2015.2467411

640 Xiu, P., Chai, F., Shi, L., Xue, H., & Chao, Y. (2010). A census of eddy activities in the South China Sea during  
641 1993–2007. *Journal of Geophysical Research: Oceans*, 115(C3). C03012, doi:10.1029/2009JC005657

642 Xu, C., Shang, X. D., & Huang, R. X. (2011). Estimate of eddy energy generation/dissipation rate in the world  
643 ocean from altimetry data. *Ocean Dynamics*, 61(4), 525-541.

644 Yang, G., Wang, F., Li, Y., Lin, P., (2013). Mesoscale eddies in the northwestern subtropical Pacific Ocean:  
645 Statistical characteristics and three-dimensional structures. *Journal of Geophysical Research: Oceans*, 118(4): 1906–  
646 1923.

647 Yi, J., Du, Y., Zhou, C., Liang, F., & Yuan, M. (2015). Automatic Identification of Oceanic Multieddy Structures  
648 From Satellite Altimeter Datasets. *IEEE JSTARS*, 8(4): 1555-1563.

649 Zhai, X., Johnson, H. L., & Marshall, D. P. (2010). Significant sink of ocean-eddy energy near western boundaries.  
650 *Nature Geoscience*, 3(9), 608-612.

651 Zhang, C. H., Xi, X. L., Liu, S. T., et al. (2014). A mesoscale eddy detection method of specific intensity and scale  
652 from SSH image in the South China Sea and the Northwest Pacific. *Science China: Earth Sciences*, 57: 1897–1906,  
653 doi: 10.1007/s11430-014-4839-y.

654 Zhang, Z., Zhang, Y., Wang, W., & Huang, R. X. (2013). Universal structure of mesoscale eddies in the ocean.  
655 *Geophysical Research Letters*, 40(14), 3677-3681. doi: 10.1002/grl.50736.

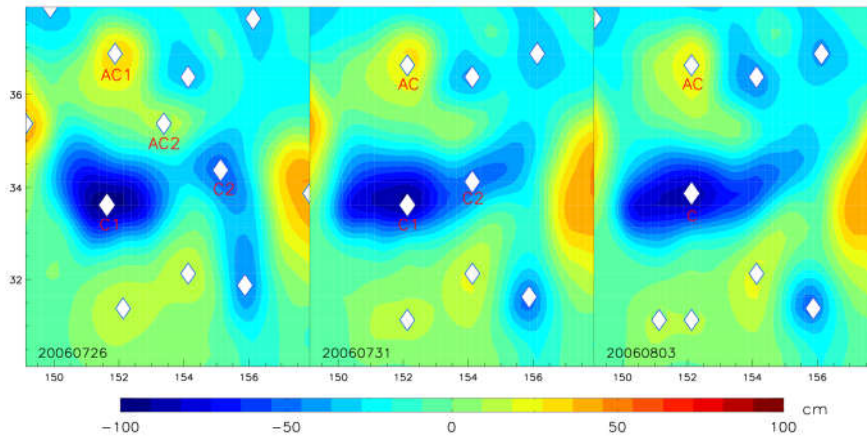
656

657

658 Table 1. The census of long-lived eddies, where “Amp” represents the amplitude threshold used in eddy detection;  
 659 and “C” and “AC,” respectively, represent cyclonic and anticyclonic eddies.

Amp	AC (>100 d)	C (>100 d)	AC (>400 d)	C (>400 d)
1 cm	7290	3627	198	22
3 cm	7118	3550	194	21

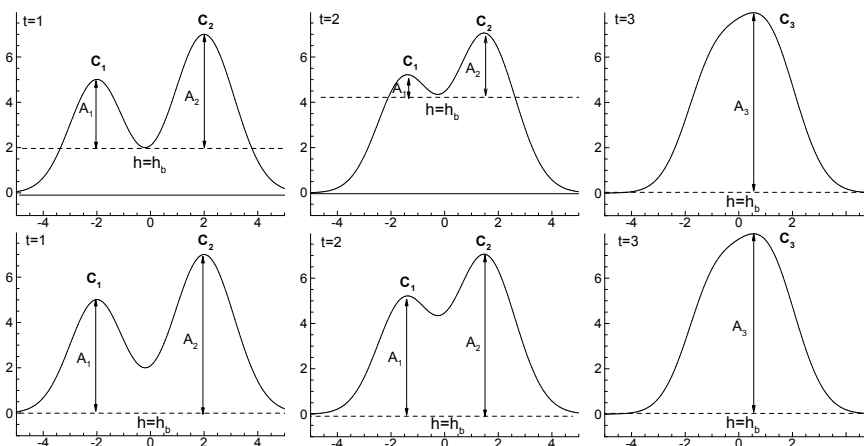
660



661

662 Figure 1. The evolutions of amplitudes and areas of eddies from July 5 to August 3, 2006 (after Li et al. 2014),  
 663 where the background field shows SLA, and white dots mark eddy centers. Two anticyclonic eddies AC1 and  
 664 AC2 merged into a single eddy on July 31, 2006. And, two cyclonic eddies C1 and C2 merged into a single one on  
 665 August 3, 2006.

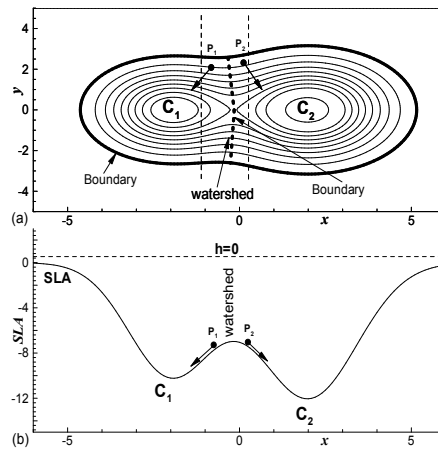
666



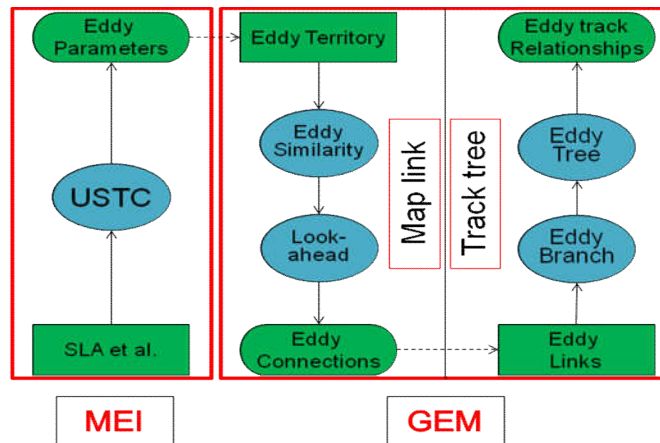
667

668 Figure 2. Top panels: Time evolution of two merging eddies revealed by the mononuclear eddy identification  
 669 without segmentation. Bottom panels: Time evolution of two merging eddies revealed by the mononuclear eddy

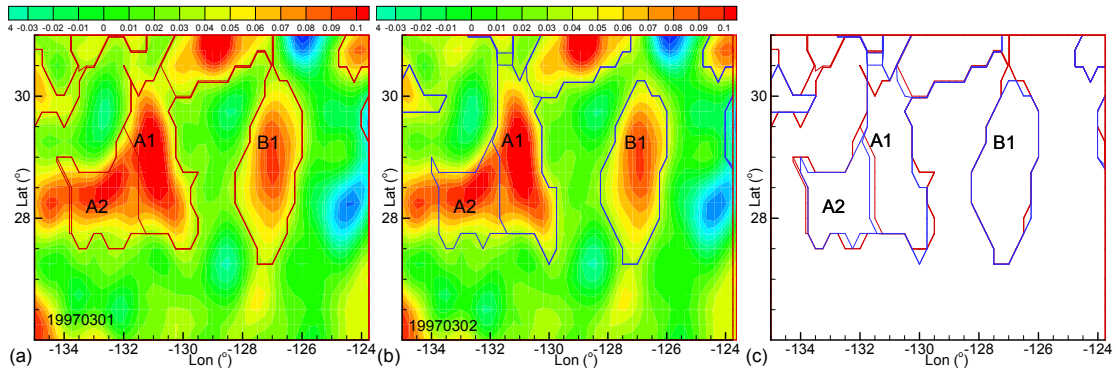
670 identification with segmentation. The  $h$  represents background SLA value,  $A$  represents amplitude of eddy,  
 671 and  $t$  represents the map at different time.



672  
 673 Figure 3. (a) Watershed as the natural division of eddies  $C_1$  and  $C_2$  from top view, where contours represent SLA. (b)  
 674 The particles  $P_1$  and  $P_2$  on the watershed flow downward to the eddy centres  $C_1$  and  $C_2$  from cross-section view.  
 675 After Li and Sun (2015).  
 676

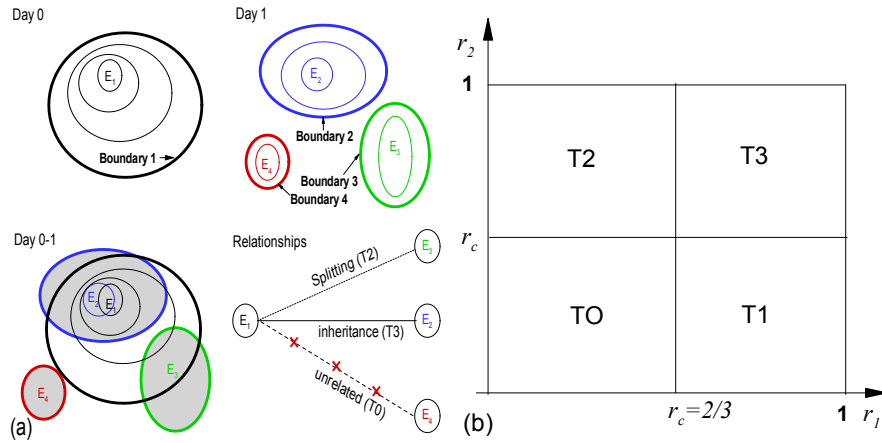


677  
 678 Figure 4. Flow chart of the systems. Mononuclear Eddy Identification (MEI) uses SLA to identify eddies via the  
 679 Universal Splitting Technology for Circulations (USTC) method. The GEM, which has two independent parts of  
 680 “Map link” and “Track tree,” then uses the previously identified eddies for tracking.  
 681  
 682



683  
 684 Figure 5. Sketch of eddy overlaps. (a) The SLA map (shading) and the boundary of eddies (red curves) on March 28,  
 685 1997, where A1, A2 and B1 represent identified eddies. (b) The SLA map (shading) and the boundary of eddies (blue  
 686 curves) on March 29, 1997. (c) The intersection of eddy territories by overlap eddy identification maps.

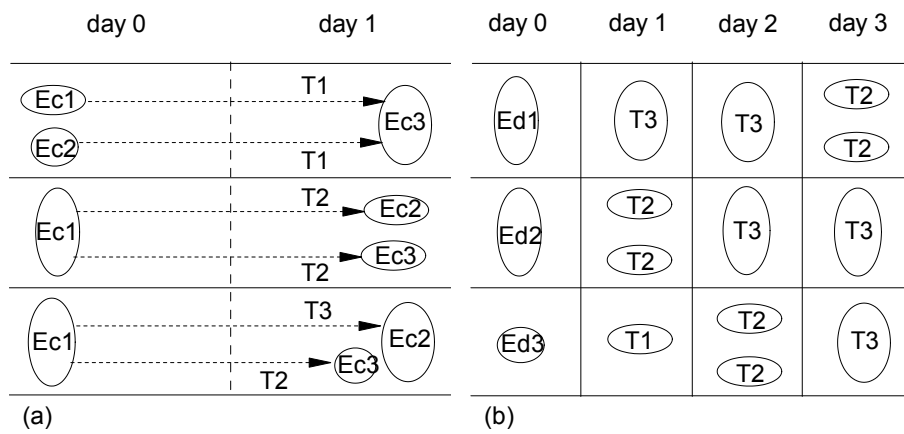
687



688  
 689 Figure 6. Sketch of eddy similarities. (a) The sketch of eddy overlaps. Eddy E<sub>1</sub> (black) is the eddy identified on day  
 690 0, where the thin contours represent the eddy parameter (e.g., the SLA value). The thick contour represents the eddy  
 691 boundary. Eddies E<sub>2</sub> (blue), E<sub>3</sub> (green) and E<sub>4</sub> (red) are identified on day 1. We consider the overlay between the two  
 692 eddies on different days to evaluate the similarity between them. (b) There are four types (T0-T3) according to the  
 693 values of  $r_1$ ,  $r_2$  and the critical value  $r_c$ .

694





695

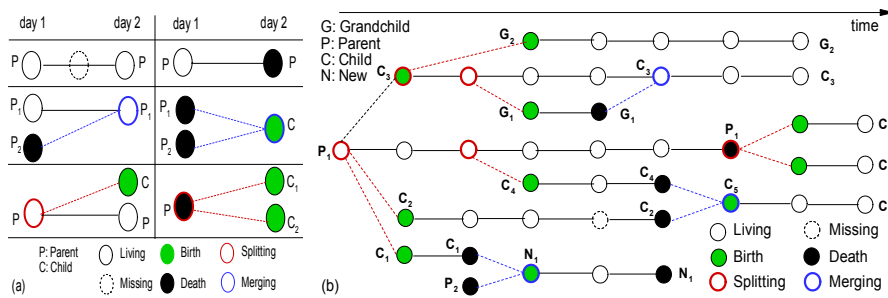
696

697

698

699

Figure 7. (a) Three typical cases of successors (T1, T2 and T3) from one day (day 0) to another (day 1). (b) The eddy at day 0 may have different successors corresponding to different numbers of “look-ahead” days, e.g., Ed1 at day 0 may have a T3 eddy on day 2, and have two T2 eddies on day 3.



700

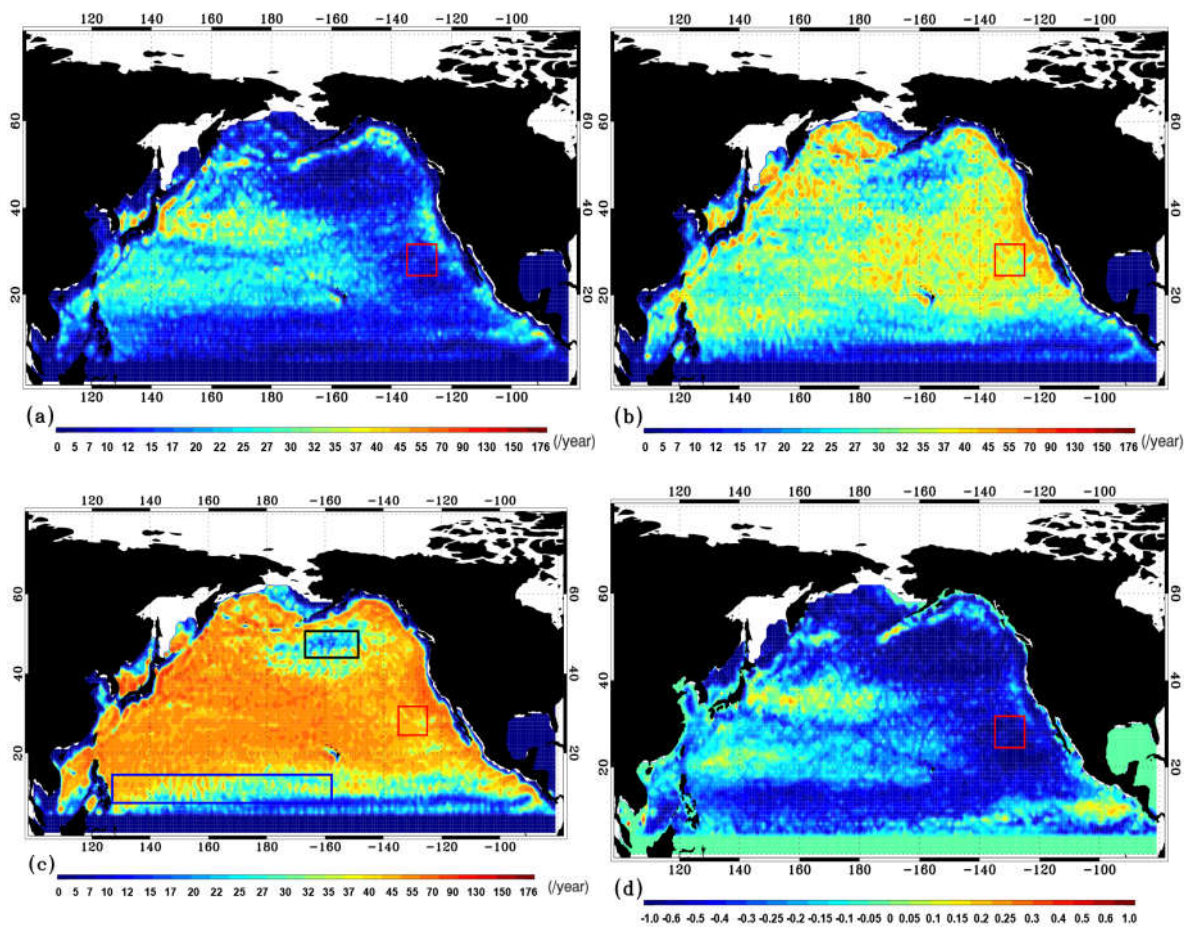
701

702

703

704

Figure 8. The logical genealogy of an ocean eddy with six states: birth, death, living, missing, splitting, and merging. (a) The logical relationships of eddies between two days. (b) The logical genealogy evolution model of an example eddy.



705

706

707

708

709

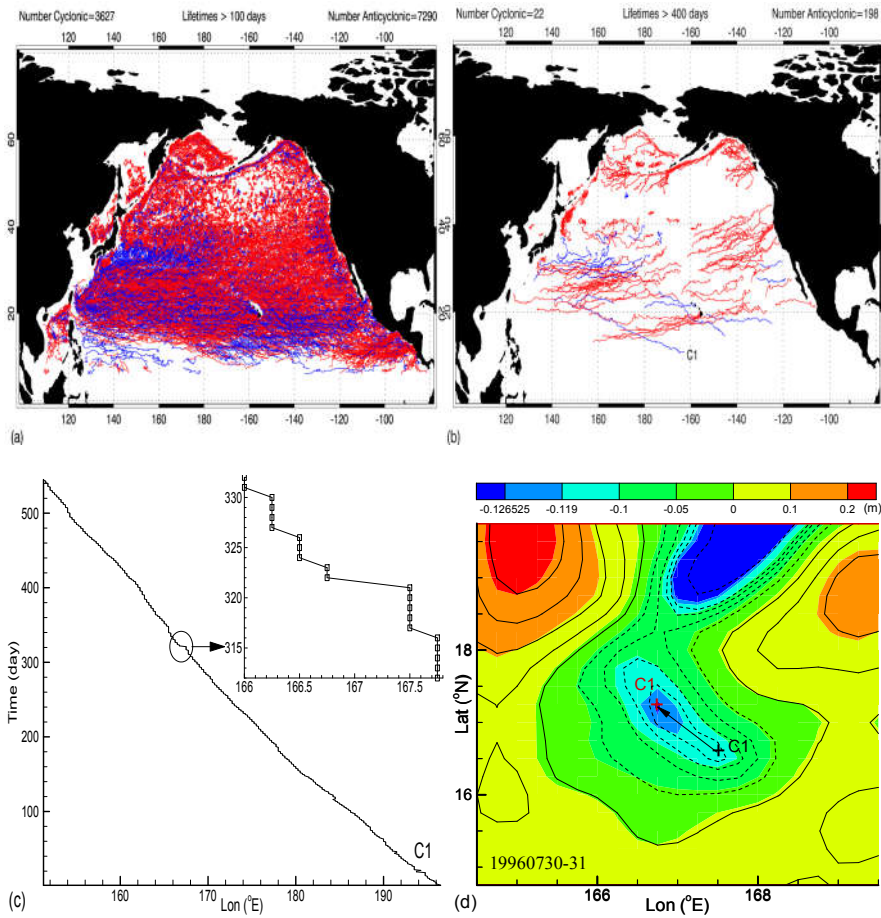
710

711

712

Figure 9 (a) The number of cyclonic eddy extrema on each  $1^\circ \times 1^\circ$  grid per year. (b) Same as (a), except for anticyclonic eddies. (c) Same as (a), except for the total number of eddies. (d) The ratios of difference in number of cyclonic and anticyclonic eddies to the total eddies (A logarithmic scale is used). The black box is the “eddy desert”, the blue box is the NEC. The red boxes are the locations of merging/splitting examples in Figure 11, where anticyclonic eddies dominated.

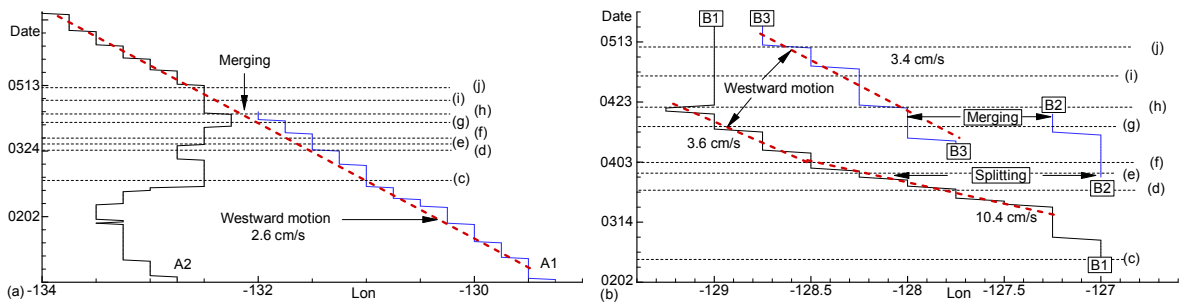
713



714

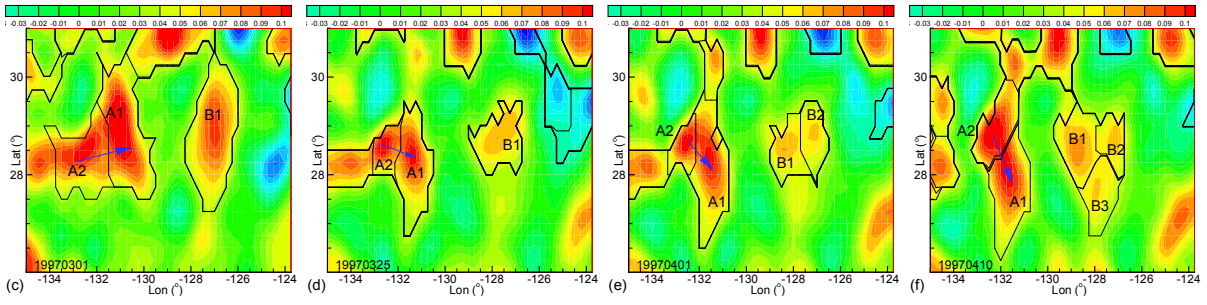
715 Figure 10. (a) Tracks of long-lived (>100 days) eddies. (b) Tracks of long-lived (>400 days) eddies. In (a) and (b),  
 716 blue color marks cyclonic eddies, and red color marks anticyclonic eddies. (c) The track of eddy C1. Note the  
 717 sudden jump from 167.5°E to 166.75°E on July 31, 1996. (d) The SLA fields on July 30 (contours) to 31 (shading),  
 718 using the same intervals for the contours and the shadings. The eddy centers are marked by a black cross (July 30)  
 719 and a red cross (July 31).

720

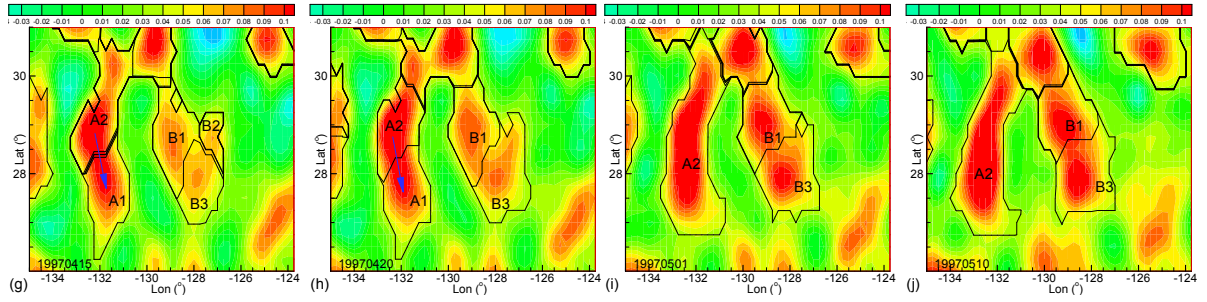


721

722



723

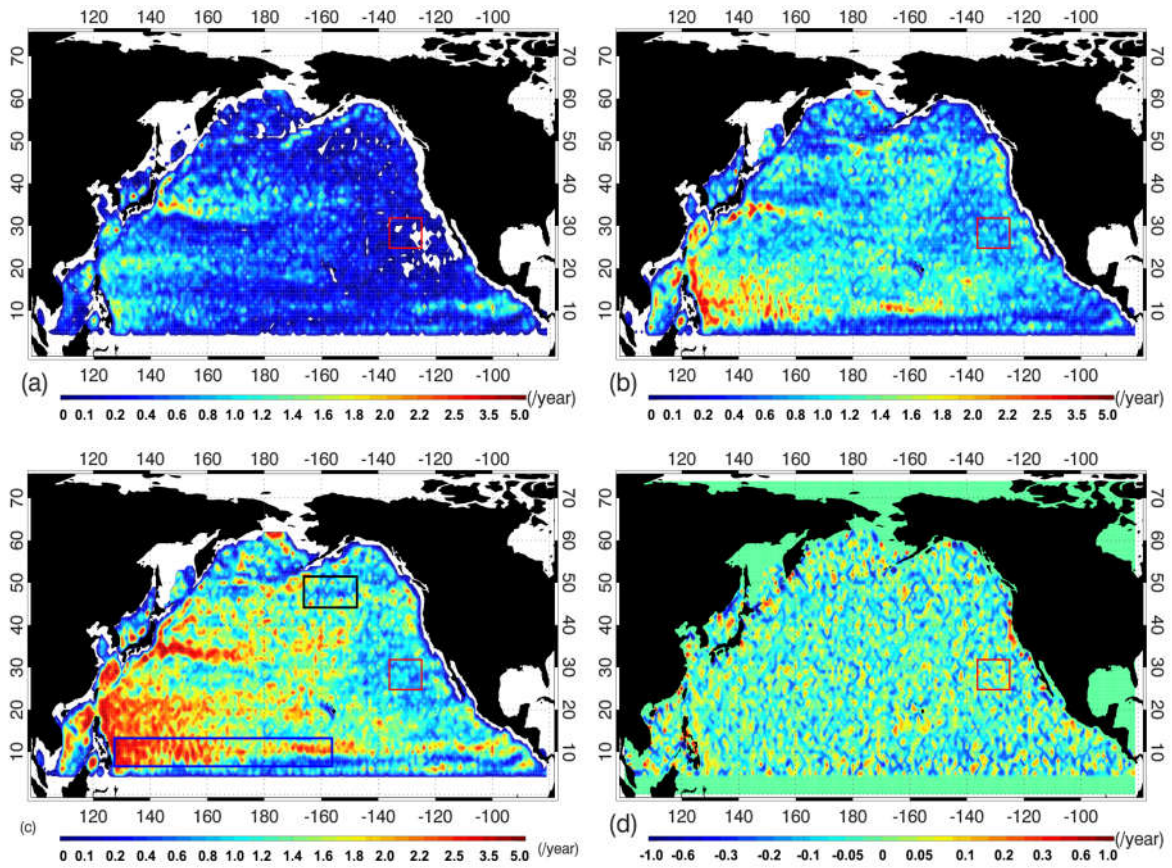


724 Figure 11. The dynamic evolutions of two groups of eddies, which are located in the red boxes in Fig. 9. (a) Two  
725 eddies, A1 and A2, approached each other, and A1 merged with eddy A2, where the blue arrows indicate that the  
726 eddy centers rotated clockwise during the merging process. (b) In the mean time, eddy B1 split into two small eddies.

727 (c)-(j) The evolutions of SLA fields and eddies. Note that eddies A1 and A2 had clockwise rotations when they  
728 approached each other, as indicated by the blue arrows in (c)-(h).

729

730



731

732

733

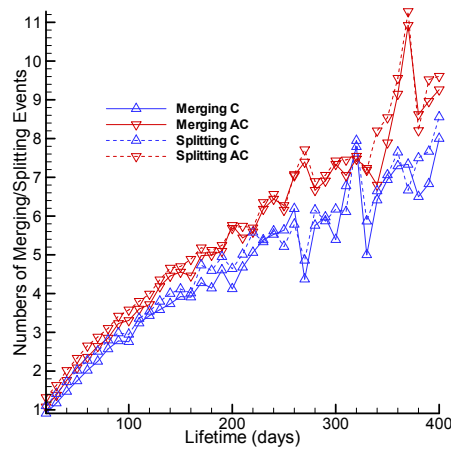
734

735

736

Figure 12. The frequencies of dynamic processes per  $1^\circ \times 1^\circ$  grid element. (a) The merging frequency for cyclonic eddies. (b) The merging frequency for anticyclonic eddies. (c) The merging frequency for all eddies. (d) The ratios of difference in number of cyclonic and anticyclonic eddies to the total eddies. The boxes are the same in Figure 9.

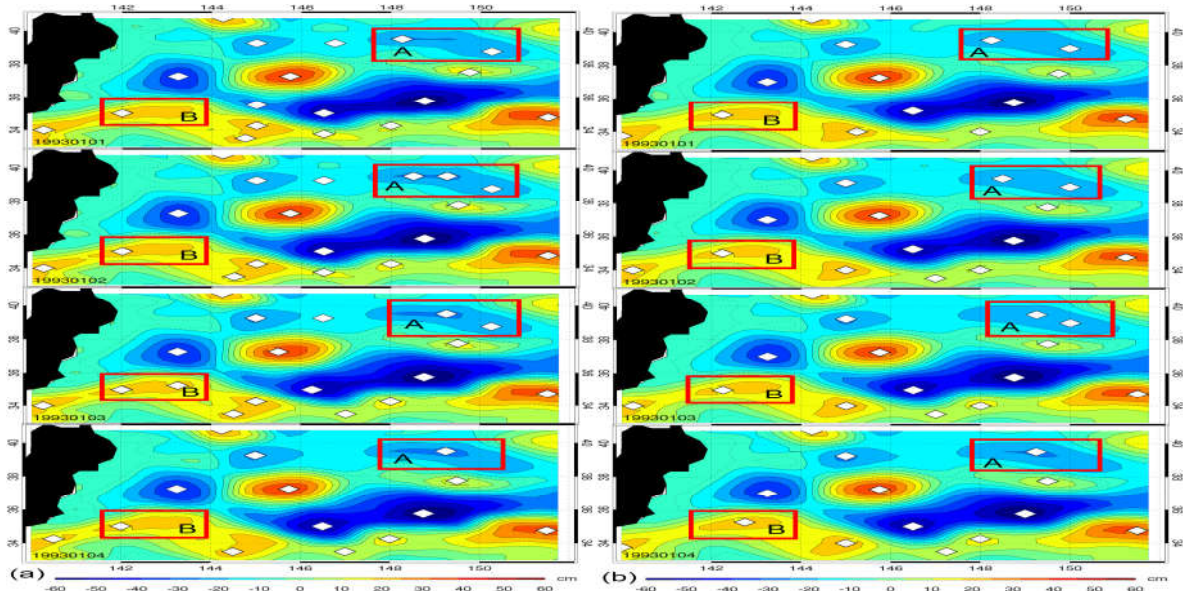
The blue box is the location of NEC, where merging frequency is high.



737

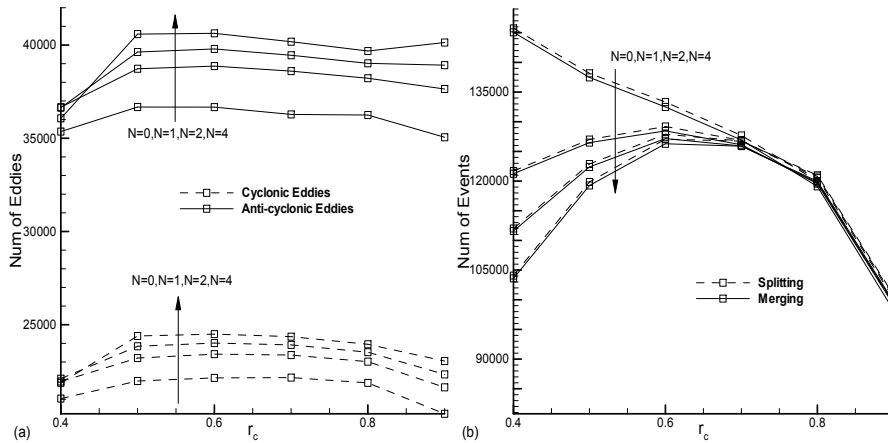
738 Figure 13. The number of merging/splitting events per eddy as function of eddy lifetime, where AC and C presents  
 739 anticyclonic and cyclonic eddies. The dynamic events are approximately linear increase with lifetime. The  
 740 merging/splitting events are more frequent for anticyclonic eddies than for cyclonic eddies.

741  
 742



743  
 744 Figure 14. Comparison of the non-smoothed (a) and smoothed SLA data (b) from January 1 to January 4, 1993,  
 745 where the color field shows SLA, white dots mark eddy centers, and two boxes A and B mark the regions sensitive  
 746 to noise. Note that small noises affected the eddy detection.

747



748  
 749 Figure 15. (a) Number of eddies (lifetime > 30 days) vs. the critical value  $r_c$  and look-ahead time  $N$ . (b) Number of  
 750 merging and splitting events vs. the critical value  $r_c$  and look-ahead time  $N$ .